SURFACE DEFORMATION OF ALPINE TERRAIN DERIVED BY PS-INSAR TECHNIQUE ON THE SIACHEN GLACIER

Junchao Shi and Ling Chang

Department of Remote Sensing, Delft University of Technology, the Netherlands.

ABSTRACT

Accumulation gain is essential for mass balance of valley glaciers in the Karakoram Himalayas. The higher elevation of this area received snowfall($>1000 \quad cm \cdot yr^{-1}$) annually, while the snowfall occupies 95% of total precipitation (75-150 $cm \cdot yr^{-1}$). Meanwhile, the air temperature ranging from -20 to -40 °C, during December-February, is also very suitable for accumulation of glacier mass. We choose ALOS/PALSAR L-band data from April, 2007, to September, 2009, in the Siachen glacier to generate the interferograms and calculate their displacements spatially and temporally. In this study, the surface deformation of upper part of the Siachen glacier located in central Karakoram is estimated by using PS-InSAR technique. Here, we implement the PS method, which uses spatial correlation of interferogram phase to find pixels with low-phase variance in the terrain. Prior knowledge of temporal variations in the deformation rate is not required for their identification. Through times series analysis of the interferograms we were able to reduce the impact of digital elevation model errors and extract the real surface change signal.

Key words: surface deformation; PS-InSAR; Siachen Glacier.

1. INTRODUCTION

The Karakoram is situated at the western end of the trans-Himalaya and is one of the largest glaciated areas outsides the polar regions, of which over 37% is covered by glaciers[1].The aggregate amount of glaciers was investigated $16.6 \times 10^3 km^2$ approximately. This study focuses on the upper part of Siachen Glacier(35.6°N 77.3°E), the eastern part of Karakoram range, it includes Teram Shehr Glacier, Lolofond Glacier and several other tributaries. Despite, the Siachen Glacier is about 74 km long, and width varying from 1 to 8 km approximately, as the longest glacier in the Karakoram and second longest in the worlds non-polar areas, the average winter snowfall is 10.5 m and temperatures can reach to -50°C. Including all tributary glaciers, the Sianchen glacier system covers 700 km^2. Therefore, the observation of its glaciological process is limited by high attitude, remote and sophisticated meteorological conditions. Given these complex

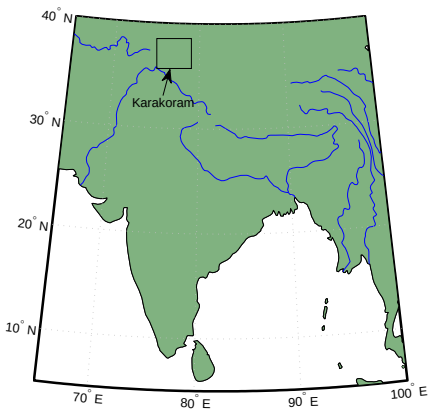

Figure 1: The general geolocation of our study area.(adapted from the imagery of Andy Proehl March, 2007.)

restraints, SAR data is an efficient source of this type glacier flow velocity estimation in general. The interferometric phase is as noted sensitive to both surface topography and coherent displacement of scatters along the radar look direction in the time between the acquisitions

of the interferometric image pairs. For glacier surface, the coherence is affected by both meteorological conditions and glacier flow velocity and generally decreases rapidly with increasing time between the acquisitions of two SAR images. Meteorological causes of decorrelation involve ice and snow melting, snowfall and wind redistribution of snow and ice. Moderate snowfall on the glaciated surface, extremely reduce temperatures and intense wind conditions give to harsh weather and climatic conditions over this region[2].

Table 1: The critical baseline of ALOS PALSAR compared with ERS/ENVISAT. ALOS −altitude = 700 km, wavelength = 23.6 cm;ERS/ENVISAT−altitude = 790 km, wavelength = 5.6 cm. Adapted from [3].

Look angle	23°	34°	41°
ALOS FBD (14 MHz)	3.6 km	$6.5km$	9.6 km
ALOS FBS (28 MHz)	7.3 km	$13.1km$	18.6 km
ERS/ENVISAT (16 MHz)	$1.1km$	2.0 km	2.9 km

2. DATASETS AND SPATIAL DECORRELATION ANALYSIS

Repeated-pass InSAR system has been proven as high accuracy level for detecting the deformation of glacier surface[4]. To estimate the deformation of glacier surface based on the spacebrone interferometry, we choose the upper part of Siachen glacier with a high relief in Karakoram. But the the longer temporal interval between selected master and slave images will result in the shifts of backscatter characteristics of surface targets; on the other hand, it is worth to keep in mind that larger spatial baseline or small the distance from antenna to surface can make phase unwrapping difficult, and exaggerate the effect of topography. Both of these factors will decorrelate the coherence during the generation of interferograms dominantly.

To obtain higher accuracy of deformation results, we implemented 12 scenes of ALOS PALSAR FBS and FBD mode for interferograms produce to monitor the ice motion from April 2007 to September of 2009 in our study. All the 12 scenes are involved in track 523, frame 0700, ascending pass (more details of all scences shown in Table.2). The usage of the L-band (236-mm wavelength) PALSAR in this case study over C-band (56-mm wavelength) are summaried as: deeper penetration of surface in less temporal decorrelation, enabling interferograms to have longer time separation[3]. Due to heavy snow cover attenuation in winter, the coherence of interferometric pairs was always not so perfect. Compared with C-band, the longer wavelength of L-band PALSAR data can be more suitable in this situation. Moreover, the critical baseline is extended by the longer wavelength (see Table.1), so that we could produce more moderate quality interferograms. In addition to these fundamental wavelength-dependent issues, PALSAR is operated in a number of different modes that could both enhance and detract from its interferometric capabilities[5]. In particular, the fine-beam dual polarization (FBD−HH/HV, 14 MHz) has $2\times$ worse range resolution than the FBS mode. While, the fine-beam single polarization (FBS−HH, 28 MHz) has $2\times$ better range resolution than most previous InSAR instruments, which further increases the critical baseline and could improve the spatial resolution of the interferograms. To make sense of the decorrelation by spatial effect, we check their relation by the function[6].

$$\rho_{spatial} = 1 - \frac{2\cos\theta R_y B_\perp}{\lambda r} \tag{1}$$

where

θ−incident angle

λ−wavelength of the radar

$B_\perp$−perpendicular baseline

R_y−ground range resolution

If we assumed that the local surface slope α is upward from horizontal plane, away from the slant direction; θ_0 is nominal incident angle away from the normal line of the local surface(calculated as 39.1°for ALOS-PALSAR modes here). Thus, we get the ground range resolution is related to the local slope by

$$R_y = \frac{c}{2B_w|\sin(\theta_0 - \alpha)|} \tag{2}$$

where c is the speed of light, and B_w is the frequency bandwidth of the the transmitted chirp signal. We can interpret that the correlation is inversely proportional to the ground range resolution from $Eq.1$. In each slant range resolution cell of a SAR image, the total scattered field is a coherent summation of radar backscattering from many scatterers within the ground range resolution cell. As the ground range resolution cell increases, the width of the main lobe of the impulse response function broaden and thus, the correlation between two SAR signals diminishes as shown in $Eq.1$.

Combined $Eq.1$ with $Eq.2$, we can get the obvious relation between spatial decorrelation and perpendicular baseline, surface slope

$$\rho_{spatial} = 1 - A \cdot B_\perp|\cot(\theta_0 - \alpha)| \tag{3}$$

where $A = c/(\lambda r B)$, a constant for a certain SAR system. As shown in Fig. 2, the correlation decreases with local slope until it approaches to the nominal incident angle, meanwhile, the increment of perpendicular baseline accelerates the reduction of the correlation.

Melting season of Siachen glacier starts beginning of May and culminates in July. There are 5 acquired scenes distributed in the melting season. We need to address that

Table 2: Ascending orbit data processed for Siachen glacier(track 523,frame 0700)

Date	Orbit	Sensor/Mode	Polarization	f_{DC} (Hz)
20070423	06632	ALOS PALSAR/FBS	HH	-141.38
20070608	07303	ALOS PALSAR/FBD	HH/HV	93.93
20070724	07974	ALOS PALSAR/FBD	HH/HV	97.85
20080124	10658	ALOS PALSAR/FBS	HH	68.72
20080310	11329	ALOS PALSAR/FBS	HH	46.25
20080425	12000	ALOS PALSAR/FBD	HH/HV	88.04
20080610	12671	ALOS PALSAR/FBD	HH/HV	98.57
20081211	15355	ALOS PALSAR/FBS	HH	67.81
20090126	16026	ALOS PALSAR/FBS	HH	68.07
20090613	18039	ALOS PALSAR/FBD	HH/HV	97.89
20090729	18071	ALOS PALSAR/FBD	HH/HV	102.75
20090913	19381	ALOS PALSAR/FBD	H/HV	83.29

Table 3: The specifications of chosen ALOS PALSAR pairs for upper part of Siachen glacier in this study.

Interferogram pairs	B_t (days)	$B_\perp$ (m)	$B_\parallel$ (m)	B_h (m)	B_v (m)	B (m)	look angle (°)	incident angle (°)
20070423-m	-414	-3319.8	-2544.7	-4177.9	206.2	4183.1	34.6	39.1
20070608-m	-368	-2630.2	-1646.2	-3099.7	-140.9	3103	34.6	39.1
20070724-m	-322	-2333.7	-1907	-3004.1	242.1	3013.9	34.6	39.1
20080124-m	-138	-1185.1	-902.1	-1487.8	68.4	1489.5	34.6	39.1
20080310-m	-92	-713	-706.9	-988.5	176.2	1004.2	34.6	39.1
20080425-m	-46	66.9	11	61.3	29	67.8	34.6	39.1
20081211-m	184	-4559	-3356.8	-5659	169.8	5661.6	34.6	39.1
20090126-m	230	-4246.4	-3228.6	-5328.9	242	5334.5	34.6	39.1
20090613-m	368	-3613.2	368	-2619.6	-4461.8	101	34.6	39.1
20090729-m	414	-3723	-2649.9	-4569.3	63.5	4569.9	34.6	39.1
20090913-m	460	-3262.3	-2382.3	-4038.2	105.2	4039.7	34.6	39.1

the coherence of interferograms will be decreased by this summer melt process. A 46-day repeat cycle provides a strong sensitivity to displacement, with one interferometric fringe roughly equivalent to 11.8 cm in the LOS direction.

Here, we generate the graph of perpendicular baseline versus time for these twelve acquisitions (see Fig. 3). All images were aligned to the master 12671 FBS so that any interferometric combination could be constructed. Another issue indicated in this figure is about Doppler frequency shifted by squint angle and relevant extra decorrelation. We checked that the PRF of all the images is between 1500 and 2500 Hz. The mean Doppler centroid (values detailed in Table. 2) of the images is 87 Hz, which is a small fraction of the PRF of 1500 Hz. The maximum difference from the mean is only 53 Hz, so there is nearly complete overlap of the Doppler spectra.

Finally, we have taken into account the precision of ALOS interferometry using SAR images from the high-bandwidth mode (28-MHz FBS), the lower bandwidth mode (14-MHz FBD), as well as mixed-mode interferograms. Above all, the critical baseline of ALOS is 6.5

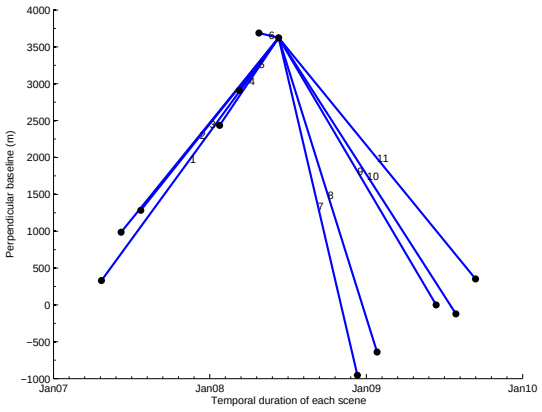

Figure 3: The time series of interferograms based on one single master image acqiured by July 10, 2008.

km for the FBD−FBD interferometry and 13 km for the FBS−FBS interferometry. None of our possible interfer-

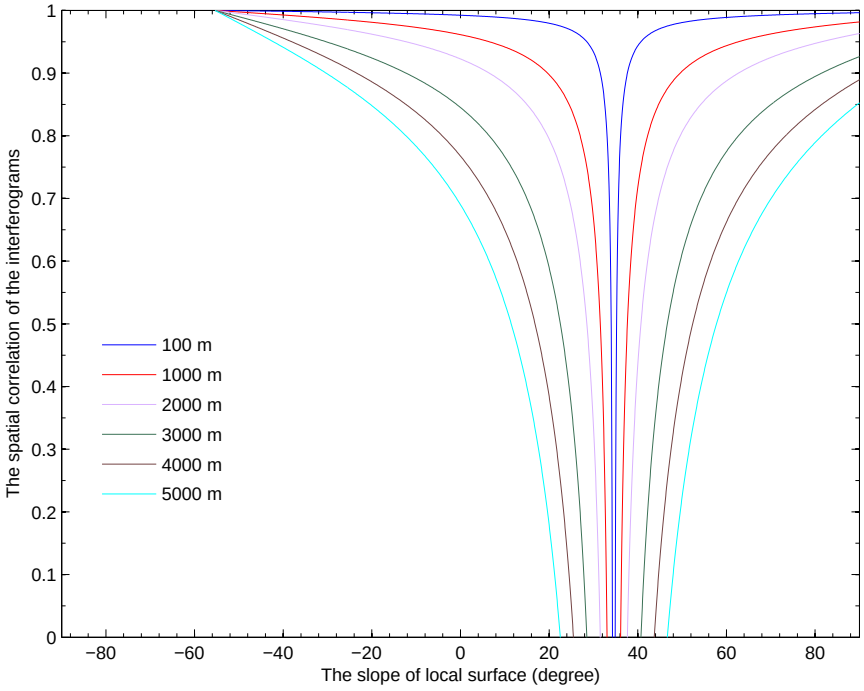

Figure 2: Spatial decorrelation with a sequence of perpendicular baselines variate with local surface slope.

ometric baselines exceeded these ranges, even one data have baseline less than 100 m. Therefore, baseline decorrelation is not an issue with ALOS. However, errors due to inaccurate topographic phase can dominate interferometric pairs with baselines longer than about 0.2 km. Therefore, either a shorter baseline must be used for measuring deformation or the accuracy of the global topographic grids must be improved. Moderate-baseline (1 km) ALOS interferograms could be used to improve the accuracy of SRTM topography.

3. DEFORMATION ESTIMATES OF THE GLACIER SURFACE IN LOS DIRECTION

Considering these factors above, we analyzed the perpendicular baseline before the co-registration and unwrapped phase generation. Then, we utilize the Persistent scatterers (PS) InSAR method, which considered the phase of the one pixel was determined by one consistent point scatterer. The principle improvement of Persistent scatterers (PS) InSAR is that it overcomes the decorrelation problem by identifying resolution elements whose echo is dominated by a single scatterer within the resolution pixel in a series of interferograms. Finally, the decorrelation of each pixel could be decreased relatively after this procedure. In practice, we select the scene of 20080610 as the only main master image, considering the Doppler centroid differences and spatial baseline, temporal baseline synthetically. Furthermore, pixels are multi-looked 5

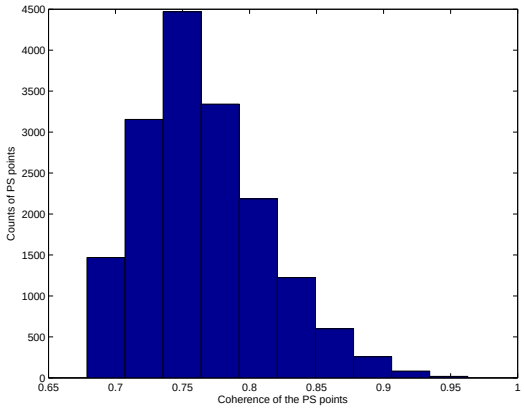

Figure 4: The quality of the final selected PS points after subtract these noise items.

times in range and 15 times in azimuth. Given, the limitation of spatial baseline, temporal separation and relevant backscatter characteristics changes of the glacier surface, we set criteria the performance of interferograms whose coherence is greater than 0.3. This may also result in more possible PS pixels for all the 11 interferograms correlated slave with masters matched in the PS selection step. Another issue in the coregistration is to avoid the some interferograms failed if only used the old cross-

relation of amplitude method. When we processed the coregistration, the amplitude based algorithm was used to estimate the offsets in position between pairs of images with good correlation.

Then, we concentrated on preparing for the PS pixels generation using the phase stabilities calculation and amplitude. Through this way, we remained identified probable PS pixels and rejected those pixels that tended to be prevalent only in certain interferograms and that may be dominated by scatterers in neighbor pixels.In Fig. 4, we summarize the the quality of the final PS points. Most of their coherences are greater than 0.6 to confirm the improvement of the series procedures for the conventional InSAR failed case. So, we processed the unwrapping depending on the optimization routines of SNAPHU[7]. After the unwrapping procedure, we diminish such as look angle error, squint angle error, and extract the displacement in LOS direction by participated PS pixels for each interferogram[8]. Consequently, we calculate the LOS (line of sight) velocity maps based on the master image during 2007-2009.(see in Fig.5)

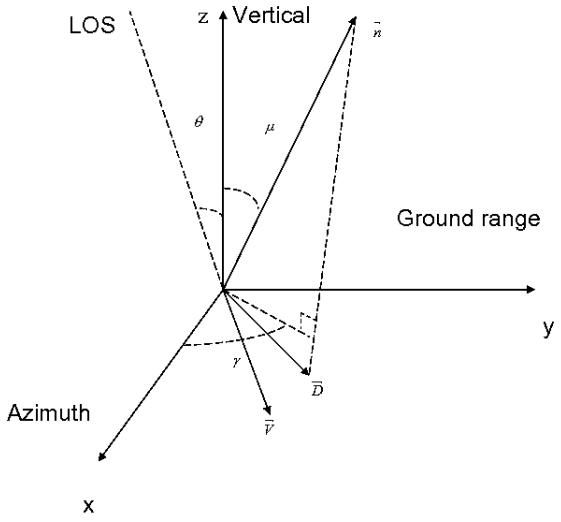

Figure 6: The geometry projecting LOS displacement to glacier surface

4. INTERPRETATION OF VELOCITIES COUPLED WITH GLACIER DYNAMICS

After a series of processing, such as, interferograms produce and pixel phase stability estimates and PS selection, achieved in the previous section, the LOS velocity map was established. If assumed the phase information involved in each PS pixel of one interferogram, we can generally project the slant range differences in vertical direction like this(see Fig. 6).

$$-\frac{\lambda}{4\pi}\phi\cos\theta = V_{\perp} + \varepsilon \tag{4}$$

where λ is the radar wavelength, which is 23.6 cm for ALOS-PALSAR L-band radar;θ is radar incidence angle, ϕ is the unwrapped interferometric phase; $V_{\perp}$ is the vertical velocity;ε is all the related error caused by residual topographic contribution due to errors in DEM, look angle error, squint angle error, atmospheric delay and so on. This results has subtracted the phase information due to topography and other noise factors. Currently, we intend to interpret this velocity result with specific glacier dynamics.

Initially, we determine the average equilibrium line(ELA) around the altitudes betwee 5400 m and 5600m, then divide the accumulation zone from the entire glacier. It indicates that most debris-covered area of Siachen Glacier below this level is retreating rapidlyReasonable correlation levels can usually be obtained in low accumulation area(e.g.75~150 cm$\cdot yr^{-1}$), while in many high accumulation areas (e.g.$1000cm \cdot yr^{-1}$)[9].

In terms of the glacial mechanism, the steady-state of glacier exhibits uplift ($v_{\perp} > 0$) in its ablation area and subsidence in its accumulation area ($v_{\perp} < 0$) to compensate for local mass balance. In general $v_{\perp}$ is expected to be larger than $v_{\parallel}$ for valley glaciers than for ice streams. In such a steady state, the surface in the accumulation area must everywhere be sinking at a rate that balances accumulation, and conversely in the ablation zone. Thus, the vertical velocity at the surface $v_{\perp}$, is clearly related to the net balance rate This is due to the higher mass-balance gradients and associated larger longitudinal strain rates of valley glaciers. Therefore α_G can differ from α_V by as much as 2-3°for valley glaciers.

5. CONCLUSIONS

Here, PS-InSAR calculation shows its high accuracy (mm level) to determine ice movement in the slant-range direction and vertical direction. We produced the local maps of glacier surface deformation in time series over upper area of Sianchen glacier. It is clear that the estimated area of the Siachen Glacier and its tributaries are active, even over their upper regions where the temperature is considerably low in winter. In general, ALOS-PASAR L-band SAR data combined PS-InSAR method overcomes the lower coherence decreased by snow cover in winter, which is very potential to describe the characteristics of glacier dynamics.

Obviously, the submergence and emergence velocities are defined for any point on a glacier surface. Due to the net balance rate b_n fluctuates from year to year, they equal b_n only in the idealized steady-state situation that we have specified. In other words, if the accumulation rate consistently exceeds the submergence velocity and the ablation rate consistently. For the next step, it is potential to merge the high precise velocities results for calculating the net balance rate.

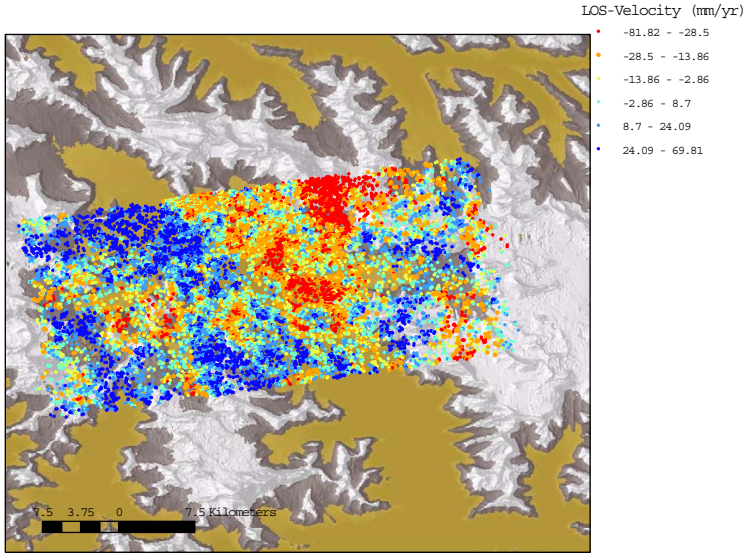

Figure 5: Mean LOS velocity map in Siachen glacier between spring, 2007 and winter, 2009 from ascending orbit of ALOS PALSAR. The velocity are related to the mean velocity of PS pixels on the upper part of Siachen glacier.

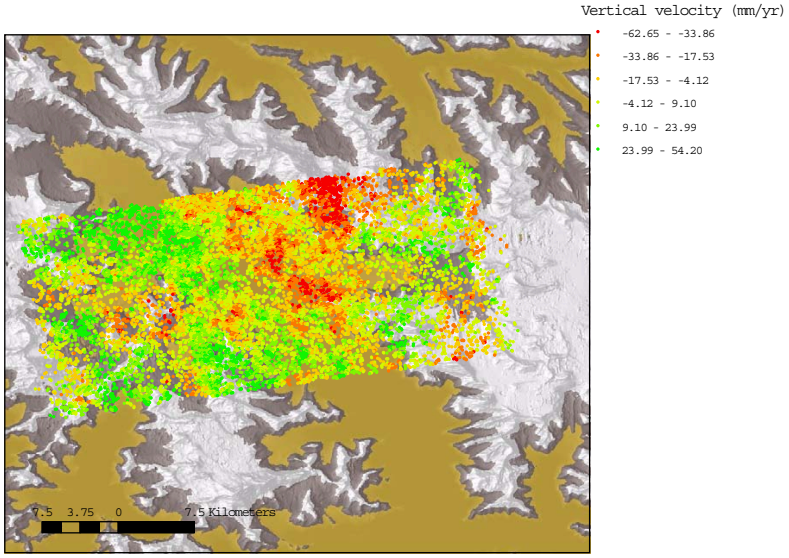

Figure 7: The mean vertical velocities of Siachen Glacier during 2007-2009.

ACKNOWLEDGEMENTS

We thank that Andy Hooper gives quite constructive comments on the processing of StaMPS method. This research was founded by the European Commission (Call FP7-ENV-2007-1 grant 212921) as part of the CEOP-AEGIS project (www.ceop-aegis.org/) coordinated by the Universit de Strasbourg. All the ALOS-PALSAR data were provided by ESA.

REFERENCES

[1] L. Copland, S. Pope, M.P. Bishop, J.F. Shroder, P. Clendon, A. Bush, U. Kamp, Y.B. Seong, and L.A. Owen. Glacier velocities across the central karakoram. *Annals of Glaciology*, 50(52):41–49, 2009.

[2] AP Dimri and SK Dash. Winter temperature and precipitation trends in the siachen glacier. *Current science*, 98(12):1620, 2010.

[3] D.T. Sandwell, D. Myer, R. Mellors, M. Shimada, B. Brooks, and J. Foster. Accuracy and resolution of alos interferometry: Vector deformation maps of the father's day intrusion at kilauea. *Geoscience and Remote Sensing, IEEE Transactions on*, 46(11):3524–3534, 2008.

[4] I. Joughin, R. Kwok, and M. Fahnestock. Estimation of ice-sheet motion using satellite radar interferometry: method and error analysis with application to humboldt glacier, greenland. *Journal of Glaciology*, 42(142):564–575, 1996.

[5] M. Shimada, O. Isoguchi, T. Tadono, R. Higuchi, and K. Isono. Palsar calval summary and update 2007. In *Geoscience and Remote Sensing Symposium, 2007. IGARSS 2007. IEEE International*, pages 3593–3596. IEEE, 2007.

[6] H.A. Zebker and J. Villasenor. Decorrelation in interferometric radar echoes. *Geoscience and Remote Sensing, IEEE Transactions on*, 30(5):950–959, 1992.

[7] CW Chen and HA Zebker. Two-dimensional phase unwrapping with statistical models for nonlinear optimization. In *Geoscience and Remote Sensing Symposium, 2000. Proceedings. IGARSS 2000. IEEE*

2000 International, volume 7, pages 3213–3215. IEEE, 2000.

[8] A. Hooper, H. Zebker, P. Segall, and B. Kampes. A new method for measuring deformation on volcanoes and other natural terrains using insar persistent scatterers. *Geophysical Research Letters*, 31(23):5, 2004.

[9] MR Bhutiyani. Mass-balance studies on siachen glacier in the nubra valley, karakorum himalaya, india. *Journal of Glaciology*, 45(149):112–118, 1999.